

High Resolution Observation of the Noble-Metal/ZnO-QDs/rGO Ternary System Using Ultra-Thin SiN_x Window *in situ* Liquid Cell Scanning Electron Microscopy

Yang Liu,^{ab} Linfeng Sheng,^a Muhammad Abdullah,^a Xing Shen,^c Ying He,^a Juan Liu^d and Xin Chen^{*a}

^a The Key Laboratory for Ultrafine Materials of Ministry of Education, Shanghai Key Laboratory of Advanced Polymeric Materials, School of Materials Science and Engineering, East China University of Science and Technology, Shanghai 200237, China.

^b Lisiyi Instrument & Equipment Co., Ltd., Shaoxing, 312000, China.

^c Ruijin Hospital Proton Therapy Center Shanghai Jiaotong University School of Medicine, Pancreatic Disease Center, Ruijin Hospital, School of Medicine, Shanghai Jiaotong University, Shanghai 201800, China.

^d Research Center of Analysis and Test of East China University of Science and Technology, Shanghai 200237, China.

*Corresponding author. Email: xinchen73@ecust.edu.cn.

Preparation of Ag/ZnO QDs/rGO Oleic Acid Emulsion Sample

Oleic acid (OA) was obtained from Shanghai Macklin Biochemical Technology Co., Ltd (Shanghai, China), while Ag NPs solution (Ag, cetyltrimethylammonium bromide (CTAB) modified) was purchased from Nanoseedz Co., Ltd (Hongkong, China).

Firstly, CTAB (20 mg) was added to deionized water (10 mL) and sonicated for 10 minutes to obtain a clear 2 mg mL⁻¹ CTAB solution. After that, OA (0.9 g) was added to the CTAB solution, and the OA emulsion was obtained after ultrasonic treatment at 25 °C for 30 minutes. Then, ZnO QDs/rGO colloidal solution (100 μL, 0.18 mg mL⁻¹) and Ag NPs solution (100 μL) were mixed and treated with ultrasound for 30 minutes to get Ag/ZnO QDs/rGO composite solution. Finally, OA (50 μL) emulsion and Ag/ZnO QDs/rGO solution (100 μL) were mixed and sonicated for 30 minutes to obtain Ag/ZnO QDs/rGO OA emulsion composite solution sample.

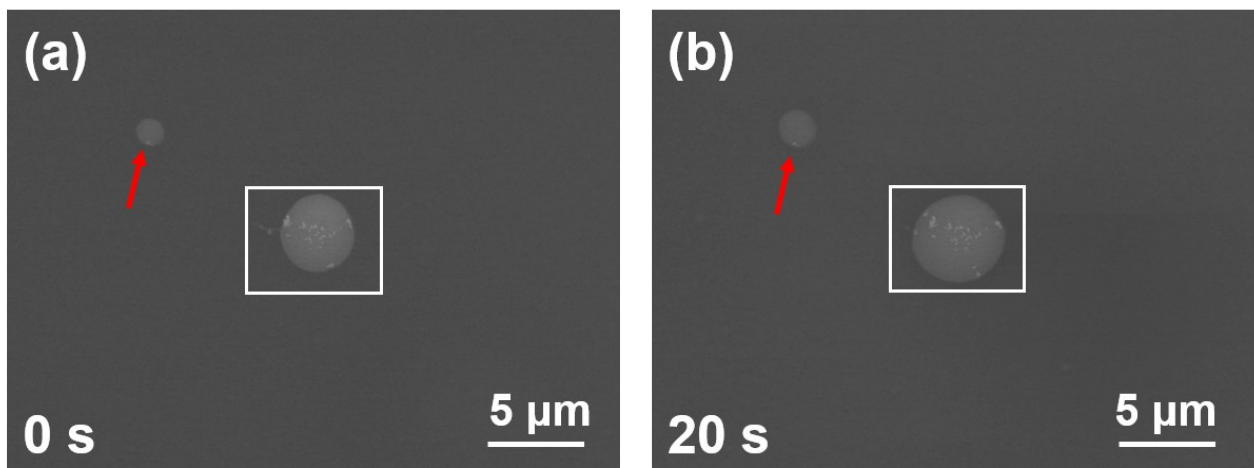


Fig. S1. *In situ* observation of droplets growths in the Au/ZnO QDs/rGO system at a low magnification under a 50 nm SiN_x window. The enlarged images inside the white boxes in (a) and (b) are shown as Fig. 4 in the main manuscript. The droplets indicated by the red arrows also underwent growth and shape change processes.

Supporting Data of LC-SEM Observation with S4800 FESEM

The supporting data of the observations made with S4800 FESEM is shown in Fig. S1-S6.

In Fig. S1(a) and S1(b), the droplet indicated by the red arrow also experienced droplet growth, but compared to the larger droplet in the white box, the growth of this smaller droplet is more isotropic.

To study the particle motions of the liquid solution sample in more detail, further analysis is made on the sample of Fig. 4. Fig. S2(a) shows time series images of the sample area in the pink box of Fig. 4(a). It was clearly seen that Au NCs 1 to 4 pointed by the yellow arrows performed continues motions between 60-120 s. Fig. S2(b) depicts individual Au NPs in each of the four Au NCs, from which, particle motions and NC shape changes can be clearly seen. Specifically, NC 2 and 4 show folding/unfolding deformations, and NC 1 and 3 show space angle changes. Fig. S2(c) shows the motion trajectories of the NCs, obtained by measuring the positions of the representative particles in each of the NCs, as indicated by the red arrows in Fig. S2(b). There appears to be an overall horizontal motion trend, which might be related with the quicker

horizontal expansion of the droplet, which remains to be further studied. Fig. S2(d) shows the

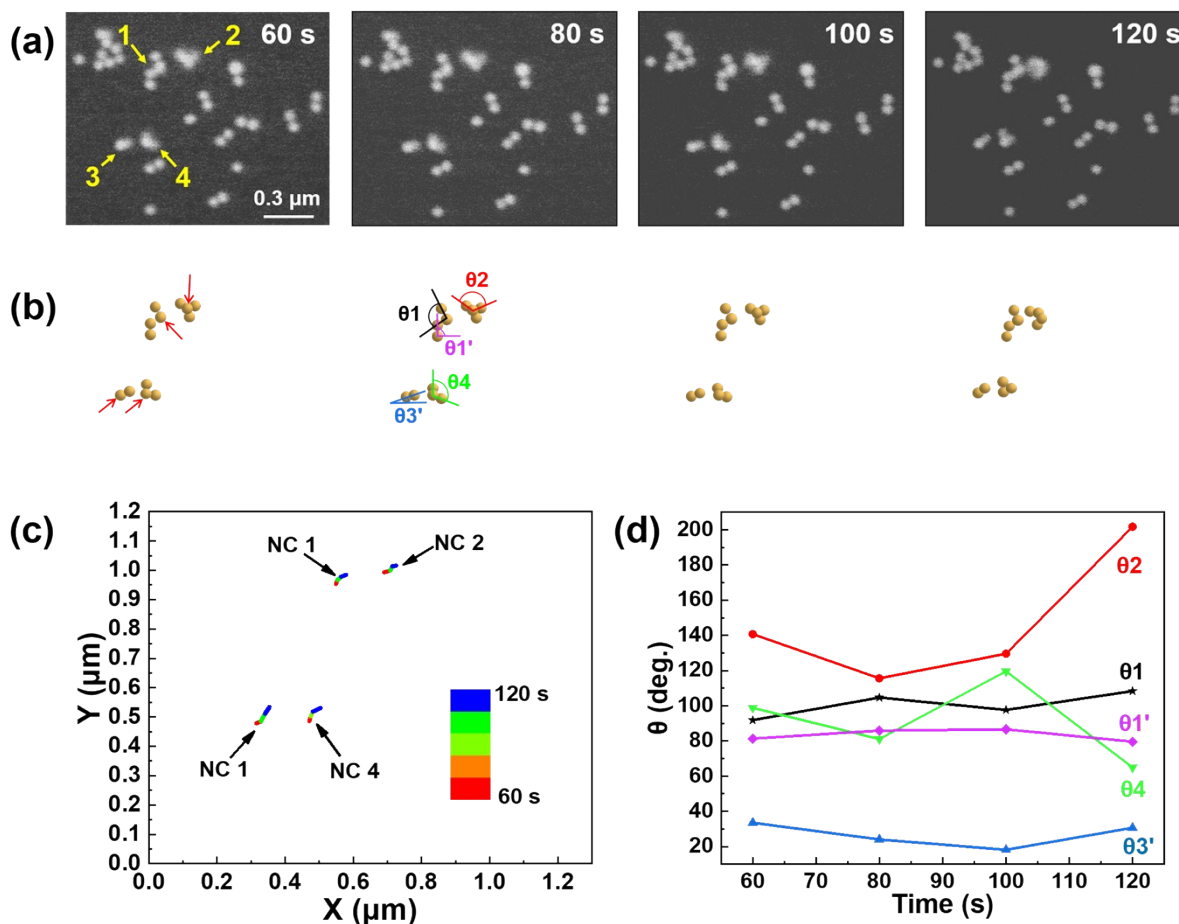


Fig. S2 *In situ* observation of the movement of Au NCs inside the pink box in Fig. 4 under BSE mode and a higher magnification. (a) Time series images with four Au NCs marked out (The time when Fig. S1(a) (Fig. 4(a)) was taken is defined as 0 s. After increasing the magnification, time series images were taken since 60 s). (b) The schematic plot of the positions of the four Au NCs indicated by the yellow arrows in (a). (c) The motion trajectories of the four Au NCs from 60 s to 120 s (Measured from the representative NPs pointed by the red arrows in (b)). (d) Angle change curves of the four Au NCs ($\theta_{1'}$ and $\theta_{3'}$ are the spatial angles between Au NCs 1 and 3 and the horizontal line, while θ_1 , θ_2 , and θ_4 are the angles between Au NP branches inside Au NCs 1, 2, and 4, respectively, as illustrated in (b)).

angle variation of Au NCs as indicated in Fig. S2(b). From Fig. S2(d), it is seen that the angle

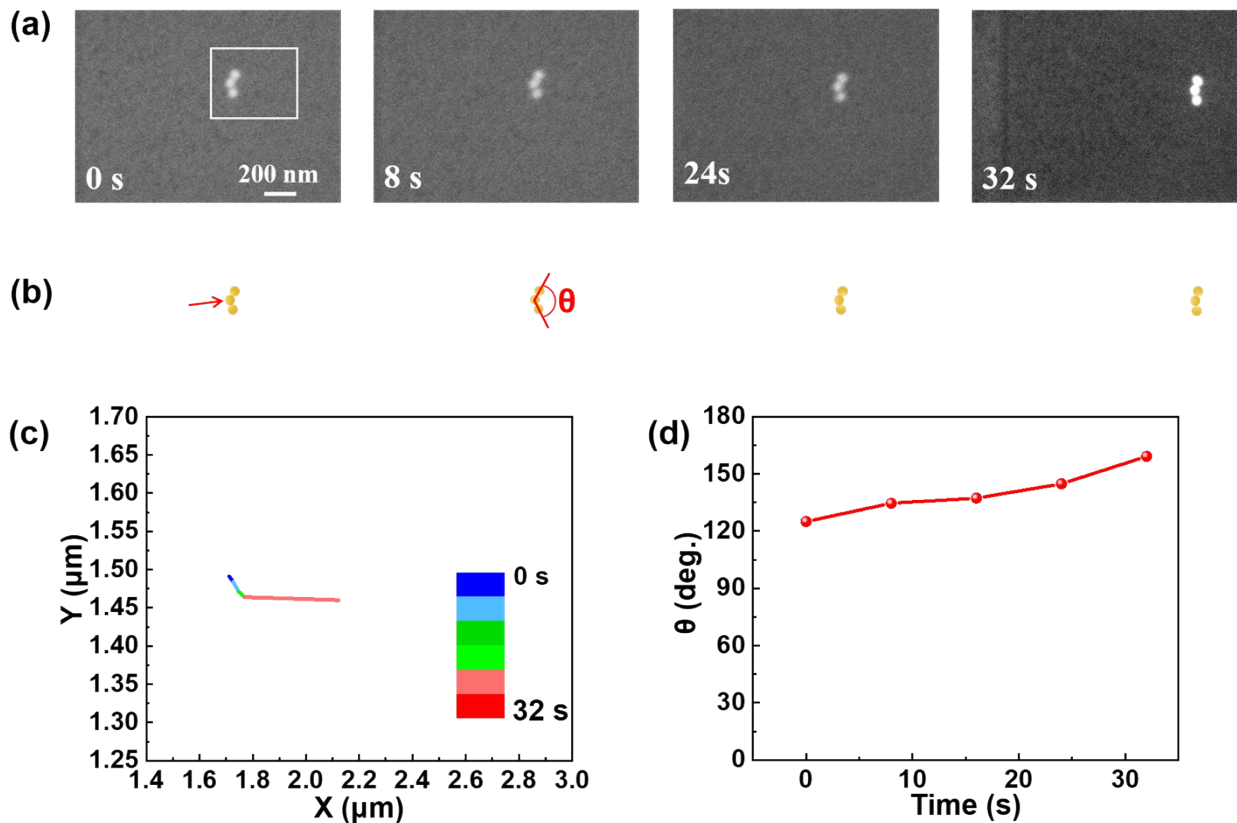


Fig. S3 *In situ* observation of the movement of an Au NC in another position of the liquid cell (under a 50 nm SiN_x window, BSE mode). (a) Time series images of the three-particle Au NC. (b) Schematic plot of the Au NC in the white box in (a). (c) Motion trajectory of the Au NC from 0 s to 32 s (Measured from the representative NP pointed by the red arrow in (b)). (d) Angle change curve of the Au NC (For the θ illustrated in (b)).

between NC 1 and the horizontal line (θ_1') first increases and then decreases, while the angle between NC 3 and the horizontal line (θ_3') shows the opposite trend. The shape change of NC 1 is not significant, and the angle change between internal particle branches (θ_1) is relatively small; however, the shape changes of NC 2 and NC 4 are large, which are accompanied with the large changes in the angle between the particle branches (θ_2 and θ_4). Overall, the changes of these angles are relatively random.

As a repeat observation, in another sample location, we observed an Au NC that performed an unfolding (straightening) shape change. The motion process of the Au NC is recorded in Fig. S3(a), and schematically illustrated in Fig. S3(b), with the motion trajectory (the representative

particle marked with a red arrow) plotted in Fig. S3(c), and the internal angle change curve plotted in Fig. S3(d). The cluster exhibits an overall horizontal rightward movement, and the angle between particle branches in the NC continued to increase with time.

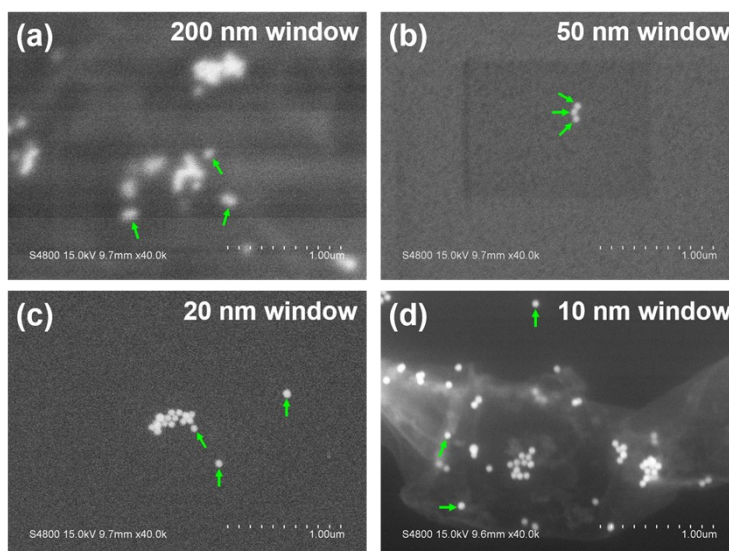


Fig. S4 LC-SEM mages of Au NPs under four different SiN_x window thicknesses for the image resolution analysis. (a)-(d) Images taken with window thicknesses of 200, 50, 20, and 10 nm, respectively. The Au NPs marked with green arrows under each window were selected for line-scan analysis to calculate the image resolution.

Fig. S4 shows LC-SEM images captured under four different thicknesses of windows. From Fig. S4(a) to S4(d), the SiN_x window thicknesses were 200, 50, 20, and 10 nm, respectively. We selected three clearest individual Au NPs (marked with green arrows) under each window for line-scan analysis to calculate the image resolution.

Fig. S5(a) and S5(b) are cross-sectional diagrams of the LC-TEM and LC-SEM liquid cells, respectively. The SiN_x window can bend due to the different internal and external pressures of the liquid cell in the vacuum environment, causing deformation and bowing up of the SiN_x window. For LC-TEM, due to the bowing up of SiN_x windows, the thickness of the liquid layer increases, resulting in a longer path of the electron beam through the liquid sample, and a loss of image resolution; for LC-SEM, although the SiN_x window also bows up, the electronic signals are collected

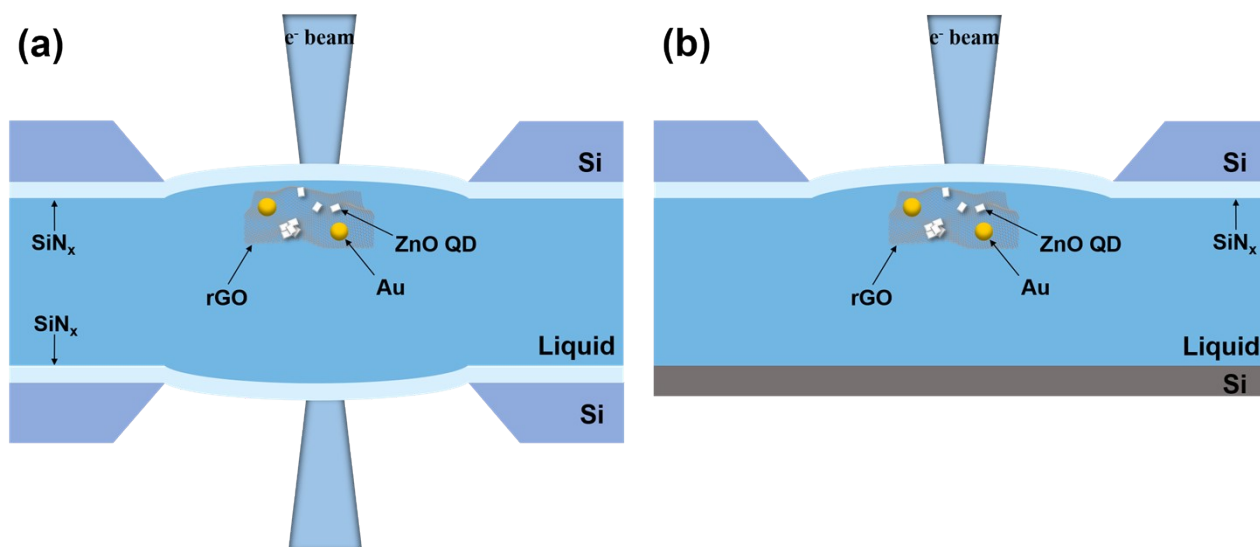


Fig. S5 Cross-sectional view of different liquid cells with bowing up SiN_x windows. (a) LC-TEM. (b) LC-SEM.

above the liquid cell, and do not need to penetrate the whole liquid layer, thus there is no loss of the image resolution for particles attached to the window.

In the vacuum chamber, the thickness and size of the SiN_x window will affect the amplitude of the bowing up. The thicker the window, the higher the strength of the window, and the smaller the amplitude of the bowing up; the larger the size of the window, the larger size of the curved window membrane, thus the larger amplitude of the bowing up. These bowing up differences will affect the LC-TEM image resolution, however, as discussed above, bowing up effect itself won't affect the LC-SEM image resolution.

On the other hand, in the process of observing ternary samples using LC-SEM, the thinner the window, the less scattering of the electron beam through the upper window, and thus the better the image resolution.

Fig. S6 is an enlarged image of the area inside the pink box in Fig. 8(a). Overall, the QD

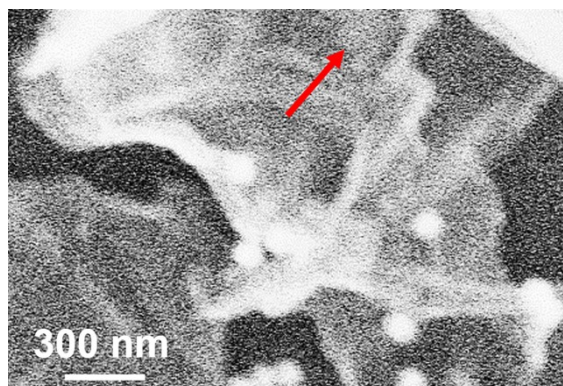


Fig. S6 Enlarged image of the region inside the pink box in Fig. 8(a). The red arrow points to a ZnO QDC in the composite.

clusters (QDCs) exhibits very dim shades, making it difficult to distinguish them from the morphology of rGO. A clearly discernable QDC is marked out with the red arrow in the figure.

***In situ* Observation of Ag/ZnO-QDs/rGO Systems with GeminiSEM500**

We conducted a comparative experiment using another type of SEM system, GeminiSEM500, to analyse the similar Ag/ZnO QDs/rGO of OA emulsion systems. Fig. S7(a) shows the OA emulsion droplets. In another location and under a higher magnification, Ag NPs, rGO nanosheet and ZnO QDs are observed in Fig. S7(b). An EDS mapping characterization on emulsion droplets is shown in Fig. S8. As the OA emulsion is mainly composed of C, H and O, the agreement of the C and O distributions in the EDS mapping diagram with the brighter regions in the SEM image confirms these brighter regions are of the OA emulsion droplets. The dark shades in the Si EDS arise from

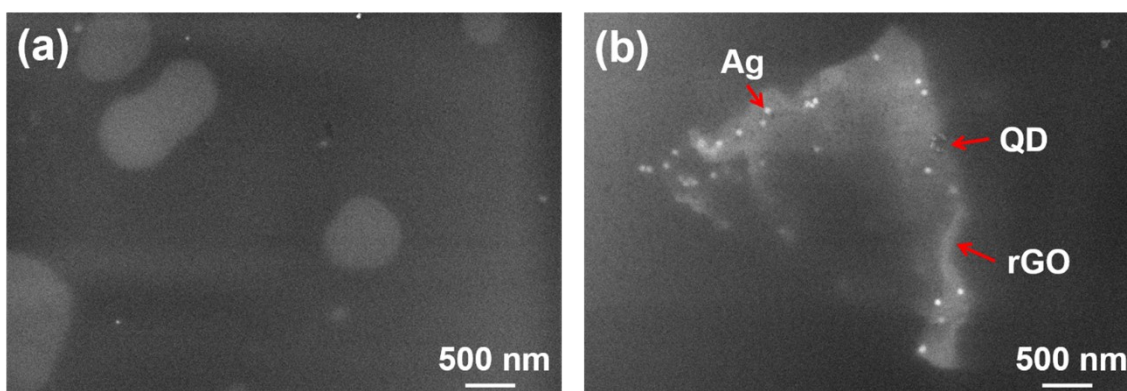


Fig. S7 LC-SEM images of an Ag/ZnO QDs/rGO ternary composite in OA emulsion, taken with GeminiSEM500, under a 20 nm SiN_x window. (a) Image of OA emulsion droplets (20 k \times). (b) Higher magnification (40 k \times) image of the Ag/ZnO QDs/rGO ternary composite in another position of the liquid cell.

the droplet blocking effect on the silicon signal from the silicon wafer substrate. It will be interesting to consider the effect of doping element in the silicon substrate, such as boron, on the EDS mapping result. However the doping level in the semiconductor wafer is generally very low, and our liquid sample here does not contain the doping elements of such as boron and phosphorous. How to avoid the interference of substrate doping element in case the liquid sample happens contain the same element, will be studied in the future.

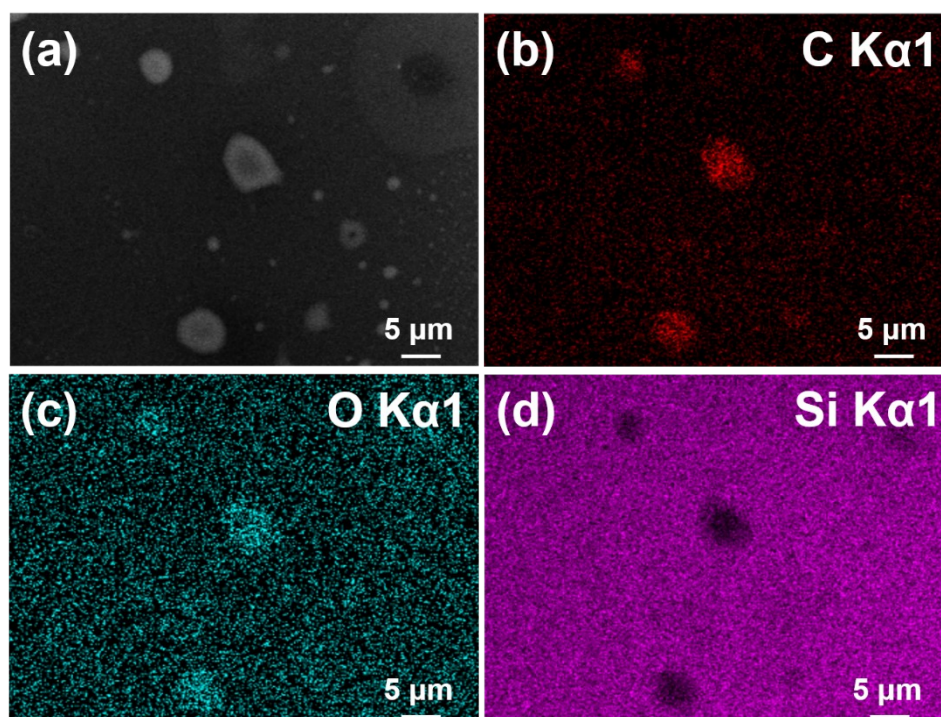


Fig. S8 EDS mapping analysis of the OA emulsion droplets. (a) LC-SEM image. (b)-(d) EDS mapping of element distributions in the sample: (b) C, (c) O, (d) Si.